Global and Planetary Change 166 (2018) 48–61

Contents lists available at ScienceDirect

Global and Planetary Change

journal homepage: www.elsevier.com/locate/gloplacha

Research article

Is the Pearl River basin, China, drying or wetting? Seasonal variations, causes and implications

Qiang Zhang[a,b,c], Jianfeng Li[d,*], Xihui Gu[e,*], Peijun Shi[a,b,c]

[a] Key Laboratory of Environmental Change and Natural Disaster, Ministry of Education, Beijing Normal University, Beijing 100875, China
[b] Faculty of Geographical Science, Academy of Disaster Reduction and Emergency Management, Beijing Normal University, Beijing 100875, China
[c] State Key Laboratory of Earth Surface Processes and Resource Ecology, Beijing Normal University, Beijing 100875, China
[d] Department of Geography, Hong Kong Baptist University, Hong Kong, China
[e] Department of Atmospheric Science, School of Environmental Studies, China University of Geosciences, Wuhan 430074, China

ARTICLE INFO

Keywords:
Soil moisture
Seasonal variation
Climate change
Variable Infiltration Capacity model
China

ABSTRACT

Soil moisture plays crucial roles in the hydrological cycle and is also a critical link between land surface and atmosphere. The Pearl River basin (PRb) is climatically subtropical and tropical and is highly sensitive to climate changes. In this study, seasonal soil moisture changes across the PRb were analyzed using the Variable Infiltration Capacity (VIC) model forced by the gridded 0.5° × 0.5° climatic observations. Seasonal changes of soil moisture in both space and time were investigated using the Mann-Kendall trend test method. Potential influencing factors behind seasonal soil moisture changes such as precipitation and temperature were identified using the Maximum Covariance Analysis (MCA) technique. The results indicated that: (1) VIC model performs well in describing changing properties of soil moisture across the PRb; (2) Distinctly different seasonal features of soil moisture can be observed. Soil moisture in spring decreased from east to west parts of the PRb. In summer however, soil moisture was higher in east and west parts but was lower in central parts of the PRb; (3) A significant drying trend was identified over the PRb in autumn, while no significant drying trends can be detected in other seasons; (4) The increase/decrease in precipitation can generally explain the wetting/drying tendency of soil moisture. However, warming temperature contributed significantly to the drying trends and these drying trends were particularly evident during autumn and winter; (5) Significant decreasing precipitation and increasing temperature combined to trigger substantially decreasing soil moisture in autumn. In winter, warming temperature is the major reason behind decreased soil moisture although precipitation is in slightly decreasing tendency. Season variations of soil moisture and related implications for hydro-meteorological processes in the subtropical and tropical river basins over the globe should arouse considerable human concerns.

1. Introduction

Soil moisture, as an important element in hydrological cycle, is highly interactive with atmosphere, hydrosphere, and biosphere (Koster et al., 2004; Fischer et al., 2007; Cheng et al., 2015). Soil moisture takes part in land surface hydrological processes and hence significantly affects exchange of land surface fluxes, such as moisture, energy, carbon, and so on (Senevirate et al., 2010). Evapotranspiration is highly associated with the partitioning of incoming energy into latent and sensible heat fluxes controlled by soil thermal parameters regulated by soil moisture condition (Bastiaanssen, 2000). Runoff generation under rainfall events is also influenced by antecedent soil moisture, evapotranspiration, and land surface characteristics. Therefore, an accurate estimation of soil moisture is necessary to investigate other hydrological variables, such as runoff and evapotranspiration (Liang et al., 1994). Human-induced global warming accelerates the global hydrological cycles, and hence alters the statistical characteristics of hydrological variables (Ziegler et al., 2003; Li et al., 2013a; IPCC, 2013). Observational evidence and model simulations have investigated the historical and projected changes in spatiotemporal distributions of hydrological variables that have sufficient high-quality ground-based measurements, such as precipitation and temperature (e.g. Zhang et al., 2011a,b; Li et al., 2013b; Sillmann et al., 2013a,b). Existing studies of changes in hydrological variables with limited ground-based observations, such as soil moisture and evapotranspiration, are mainly based on model simulations and products of remote sensing at long-term time scale, e.g. annual and decadal, and over large spatial domains, e.g. East Asia, China, USA, etc. (e.g. Yang et al., 2009;

* Corresponding authors.
E-mail addresses: jianfengli@hkbu.edu.hk (J. Li), guxihui421@163.com (X. Gu).

https://doi.org/10.1016/j.gloplacha.2018.04.005
Received 17 July 2017; Received in revised form 17 April 2018; Accepted 30 April 2018
Available online 04 May 2018
0921-8181/

Chen et al., 2016a; Cheng et al., 2015). Nevertheless, studies on soil moisture at finer temporal and spatial scales, e.g. at a seasonal scale and in a basin, are so far limited, especially for areas in China. Regional responses of precipitation and temperature to climate change are different at different time scales. Therefore, the Intergovernmental Panel on Climate Change (IPCC) the fifth report (AR5) pointed out that more regional studies on hydrological variables such as soil moisture, evapotranspiration and streamflow are needed to understand impacts of climate change on different places of the globe (IPCC, 2013).

Soil moisture controls the water available for plants and hence influences agricultural production (Lawrence and Vandecar, 2014). Agricultural activities, such as seedling, growing, harvesting, have strong seasonality (Wang et al., 2012). Therefore, soil moisture conditions in various seasons have very different implications for agricultural production. For example, persistent soil moisture deficit in autumn can result in more significant impacts on agricultural production than that in winter. However, such seasonal variability is hardly characterized at annual or even longer time scales. Seasonal precipitation deficit, i.e. meteorological droughts, has been well investigated in different regions of China (Zhang et al., 2012a,b; Li et al., 2015), but it cannot fully represent soil moisture deficit, which directly affects agricultural production and is determined by complex hydrological processes and mechanisms associated with a number of contributing factors, such as precipitation, temperature, vegetation, and land use land cover (Chen et al., 2016a). Furthermore, the relationships between soil moisture changes and the related hydrological factors are different in different areas, making the investigations on the relationships more difficult.

A drying trend is expected over China, especially in northeastern China, under global warming as shown in studies based on various data sources (e.g. Dorigo et al., 2012; Dai, 2013; Cheng et al., 2015). In most of these studies at annual scale, no significant trends in soil moisture are detected in the Pearl River basin (PRb) located in Southern China. The PRb is the second largest river in China in terms of total discharge volume with a drainage area around 4.42×10^5 km^2 (PRWRC, 1991; Zhang et al., 2009) (Fig. 1). The PRb is dominated by tropical and subtropical climate zones and largely influenced by the summer monsoon climate with annual precipitation ranging from 1000 mm to 2000 mm, while summer precipitation accounts for 72–88%. Although water resources in the PRb are more than those in North China, the strong seasonal cycle in precipitation makes it vulnerable to droughts, such as the 2010 droughts in western PRb have caused substantial reductions in agricultural production (Yang et al., 2010). Although this seasonality in precipitation and temperature and their implications on meteorological droughts over the PRb have been investigated in previous studies (e.g. Chen et al. 2016b; Zhang et al., 2012b), the seasonality of soil moisture, which is associated with agricultural droughts, has seldom been discussed so far, largely due to limited in-situ observations. Therefore, this paper aims to 1) estimate spatiotemporal changes of soil moisture in spring, summer, autumn and winter during 1961–2010; 2) examine the relationships of changes in soil moisture with precipitation and temperature and estimate the contributions of these factors to changes in soil moisture, and 3) identify roles in precipitation and temperature in changing soil moisture in different seasons. The study can shed new light on regional responses of seasonal soil moisture changes to climate variations, and provides more direct implications on agricultural droughts and productions which are more sensitive to seasonal changes in hydrological variables.

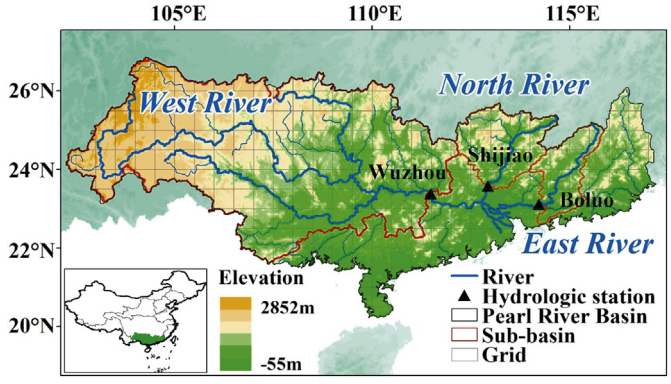

Fig. 1. The Pearl River basin and location of the hydrologic stations, including Boluo, Shijiao, and Wuzhou, which are the controlling stations of the East River, North River, and West River basins, respectively.

Table 1
The ranges and optimal values of the VIC parameters in calibration.

Parameter	Abbr.	Range	Optimal value		
			Boluo	Shijiao	Wuzhou
Infiltration parameter	b_i	0.001–1	0.19	0.56	0.60
Fraction of maximum base flow	D_s	0.001–1	0.47	0.88	0.63
Maximum velocity of base flow (mm/day)	D_m	0.001–30	14.40	21.54	16.19
Fraction of maximum soil moisture content of the third layer	W_s	0.1–1	0.38	0.40	0.37
Thickness of the first soil layer (m)	d_1	0.1–2.5	0.12	0.10	0.13
Thickness of the second soil layer (m)	d_2	0.1–2.5	0.13	0.10	0.13
Thickness of the third soil layer (m)	d_3	0.1–2.5	2.5	2.5	1.6

Table 2
Daily and monthly E and B of calibration and validation at Boluo, Shijiao, and Wuzhou.

Period	Time step	Measure	Boluo	Shijiao	Wuzhou
Calibration	Daily	E	0.84	0.76	0.89
		B	−0.07	−0.10	−0.07
	Monthly	E	0.92	0.92	0.96
		B	−0.08	−0.10	−0.06
Validation	Daily	E	0.70	0.71	0.86
		B	−0.04	−0.17	−0.12
	Monthly	E	0.81	0.88	0.93
		B	−0.04	−0.17	−0.12

2. Data

Daily precipitation and temperature data during 1961–2010 in the PRb at 0.5° × 0.5° spatial resolution were collected from the National Climate Center of China Meteorological Administration (CMA) China, to drive the VIC model. Although other observed datasets with finer resolutions are available, e.g. a dataset with 0.5° × 0.5° resolution during 1981–2008 and 0.25° × 0.25° during 1996–2006 developed by Yang et al. (2010), the lengths of these datasets are not long enough for long-term temporal changes in this study. Furthermore, previous studies have adopted 0.5° × 0.5° and coarser spatial resolutions for the PRb (e.g. Niu and Chen, 2010; Niu et al., 2014; Yan et al., 2015). Therefore, the CMA dataset can provide reasonable spatial resolution (i.e. 0.5° × 0.5°) and sufficient temporal coverage (1961–2010) to analyze temporal changes in soil moisture in this study. Daily streamflow data during 1961–2005 at Boluo, Shijiao, and Wuzhou hydrologic stations were collected from Hydrologic Yearbook to calibrate and validate the hydrological model (Fig. 1). These hydrologic stations are the controlling stations of the three major sub-basins of the PRb, i.e. the East River, the North River, and the West River basins. Wind speed was obtained from the National Centers for Environmental Prediction-National Center for Atmospheric Research (NCEP-NCAR) reanalysis (Kalnay et al., 1996).

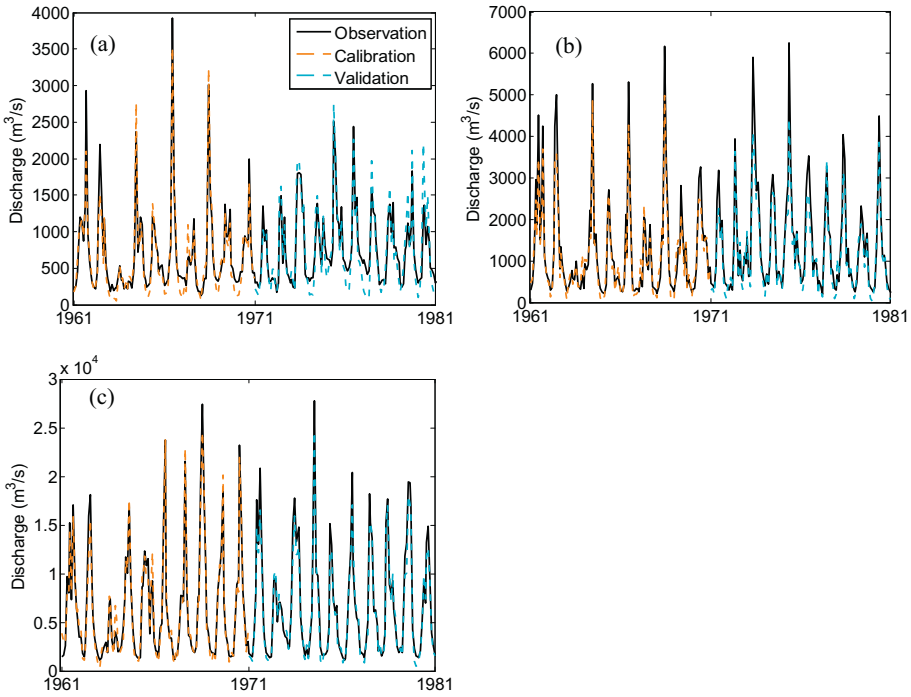

Fig. 2. Comparison of the VIC simulations against observations at the (a) Boluo, (b) Shijiao, and (c) Wuzhou during the calibration (1961–1970) and validation (1971–1980) periods.

Soil moisture from the Global Land Data Assimilation System (GLDAS) was collected to validate the VIC simulations in soil moisture (Rodell et al., 2004). GLDAS is an advanced land surface modeling system based on data assimilation techniques to incorporate satellite- and ground-based observational products with aim to generate optimal fields of land surface states and fluxes. GLDAS drives multiple and offline (not coupled to the atmosphere) land surface models and integrates a huge quantity of observational datasets at high resolutions enabled by the Land Information System (LIS) (Rui and Beaudoing, 2016). The outputs of soil moisture content in kg/m^2 in GLDAS include four layers with the depths of 0–10 cm, 10–40 cm, 40–100 cm, and 100–200 cm. The GLDAS dataset has been validated against available data from multiple data sources (e.g. Chen et al., 2013; Zhang et al., 2008), and employed for different kinds of purposes, such as data assimilation, validation, weather and climate model initialization (e.g. Lin et al., 2008; Syed et al., 2008). There are two versions of GLDAS datasets including GLDAS-1 and GLDAS-2. Compared with GLDAS-1, the GLDAS-2 has been reprocessed with updated Princeton Forcing Data and upgraded Land Information System (LIS) software, which can more effectively reduce the influences of switches of forcing data sources on outputs, such as unnatural trends and highly uncertain forcing fields. Furthermore, the GLDAS-2 outputs started from 1948, which is much earlier than the GLDAS-1 which started from 1979. Therefore, the monthly soil moisture with the depth of 0–10 cm from GLDAS-2 based on NOAH land surface model at the 0.25° × 0.25° resolution was used to validate the soil moisture simulations.

Furthermore, the Essential Climate Variables (ECV) and known as the Climate Change Initiative (CCI) soil moisture dataset reproduced by the assimilation of active, passive and combined satellite observations since 1979 was used to validate the soil moisture simulations in this study (Liu et al., 2011, 2012; Chen et al., 2016a; Feng, 2016). The active product is the output of merging scatterometer-based soil moisture data, which were derived from AMI-WS and ASCAT (Metop-A and Metop-B). The passive product merges data from SMMR, SSM/I, TMI, AMSR-E, WindSat, AMSR2, and SMOS. The combined product merges the active and the passive products with considering effects of vegetation. The layer depth of ECV soil moisture is 0.5–5 cm at the 0.25° × 0.25° resolution. For areas with dense vegetation (tropical, boreal forests), strong topography (mountains), ice cover (Greenland, Antarctica, Himalayas), a large fractional coverage of water, or extreme desert areas were masked where the soil moisture retrieval failed. The ECV combined soil moisture of version 03.2 with unit of m^3/m^3 that released recently is selected in this paper due to its improved gap filling, new data attributes, and a revision of processing algorithms and merging procedures. More details about the ECV data can be found from http://www.esa-soilmoisture-cci.org/node.

3. Methods

3.1. The variable infiltration capacity model

The Variable Infiltration Capacity (VIC) model was used to simulate daily runoff at the 0.5° × 0.5° spatial resolution over the PRb (Liang et al., 1994). The VIC model has been widely used and its performance has been well validated across the world, e.g. in Minnesota River (Cherkauer and Lettenmaier, 2003), the western United States (Shi et al., 2008), China (Wu et al., 2007), and Australia (Sivapalan et al., 1997). The VIC model is a semi-distributed macroscale hydrologic model, handling water and energy balances within a grid cell (Gao et al., 2010). In the VIC, the variable infiltration curve is used to consider the spatial heterogeneity of the runoff generation (Zhao, 1992). Saturation, excess runoff, infiltration, snow melting and soil freeze-thaw processes are considered in the VIC (Liang et al., 1994; Nijssen et al., 2001b; Dan et al., 2012). In the water balance mode, soil surface temperature is equal to air temperature, and surface energy balance is unsolved. The energy balance mode solves surface energy balance by iterative processes, which are more computational demanding. Three types of evaporations are considered in the VIC model, including canopy evaporation, vegetation transpiration, and evaporation from bare soil (Liang et al., 1994). The potential evapotranspiration (PET) is calculated from the Penman-Monteith equation based on temperatures (Shuttleworth, 1993). The actual evapotranspiration (AET) from these three types are estimated based on different formulations, e.g. formulation from Ducoudre et al. (1993), for vegetation transpiration and

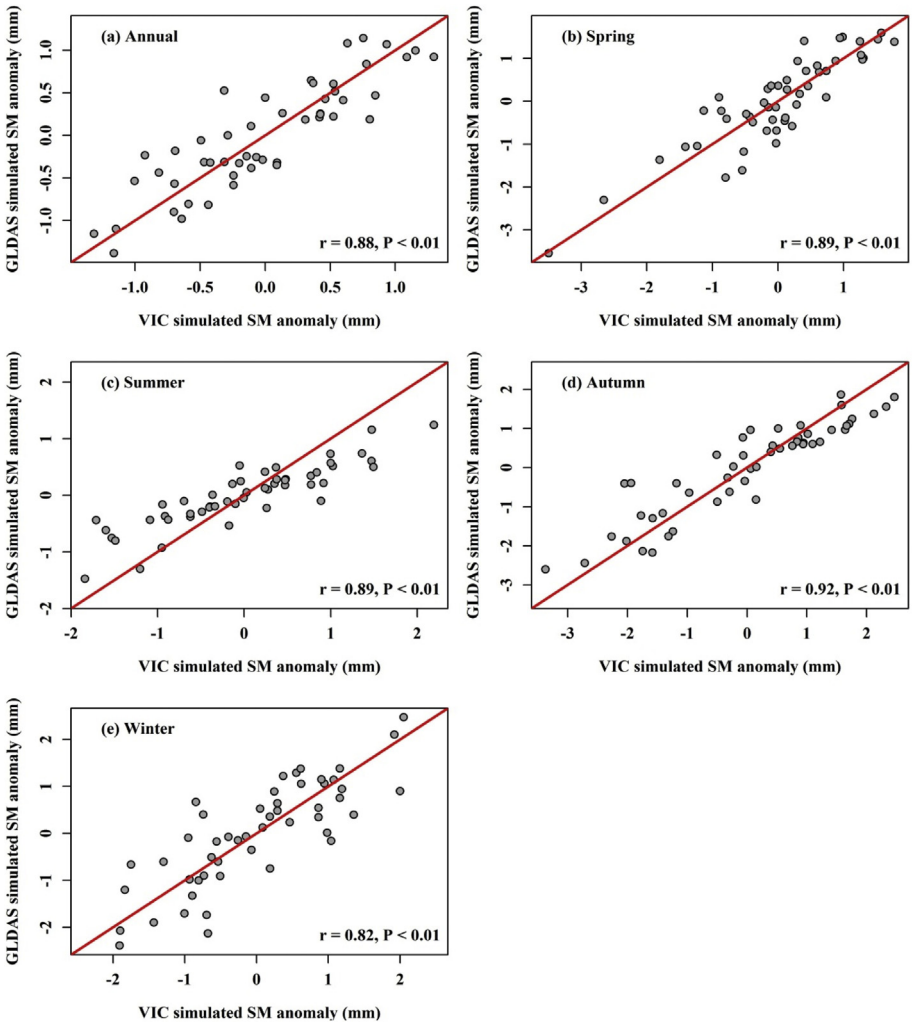

Fig. 3. Scatter plots of the areal means of soil moisture (SM) anomaly simulated by the VIC versus those of the GLDAS-2 NOAH simulations (a) of years, (b) in spring, (c) in summer, (d) in autumn, and (e) in winter during 1961–2010. The red line represents 1:1 line. In the subplots, r is the correlation, and P represents the *p* value of the correlation.

Arno formulation for soil evaporation, with consideration of parameters for different vegetation types, soil properties, soil moisture. More details of the VIC can be found in Gao et al. (2010).

The global parameters at the 0.5° × 0.5° spatial resolution generated by (Nijssen et al. 2001a, 2001b) were used to represent the land surface properties in the VIC. The soil textural parameters and soil bulk densities were derived from the Food and Agriculture Organization (FAO, 1998) combined with the World Inventory of Soil Emission Potentials pedon database (Batjes, 1995). Vegetation types were obtained from 1 km AVHRR (Advanced Very High Resolution Radiometer)-based land classification from Hansen et al. (2000). Despite these physically-derived parameters, there are seven soil parameters subject to calibration, including infiltration parameter *bi*, fraction of maximum base flow D_s, maximum velocity of base flow D_m, fraction of maximum soil moisture content of the third layer W_s, and thicknesses of the three soil layers d_1, d_2 and d_3 (Xie et al., 2007). In this study, the VIC was implemented for the East River, the North River and the West River basins with 3 soil layers at a daily time step with the water balance mode. After solving the water balance in a grid cell, the base flow and runoff are determined at the end of the time step. A routing model was employed to rout surface runoff and base flow to the outlet of grid cells then into the river channel of that basin (Lohmann et al., 1998). The routing model calculates the concentration time for runoff to the outlet of a grid cell and the channel flow in the river network (Gao et al., 2010). The within-cell routing is solved by a linear transfer function based on the internal impulse response function. Then the linearized Saint-Venant equation is used for channel routing.

The Shuffled Complex Evolution (SCE-UA) method, a global optimization procedure developed by Duan (1992, 1993), was used to calibrate VIC by optimizing the seven aforementioned parameters. Two measures were incorporated into the objective function: the Nash-Sutcliffe efficiency measure *E* (Nash and Sutcliffe, 1970) and the bias *B* (total model error divided by total observed streamflow). The objective function *F* is a weighted combination of *E* and a logarithmic function of *B* as indicated by Viney (2009).

$$F = E - 5\ |\ln(1 + B)|^{2.5} \quad (1)$$

The coefficients of this function control the severity and shape of the bias constraint penalty (Zhang et al., 2012a). The ranges of these parameters for calibration are shown in Table 1. The period of 1961–1970 was used for calibrating the VIC model, while the period of 1971–1980 was used for validating the VIC model. The PRb has been experiencing rapid economic development and widespread land use changes since the 1980s and these changes significantly affected the hydrologic conditions (Seto et al., 2002). Therefore, choosing periods before the 1980s for model calibration and validation was to minimize the effects of human activities on calibration and validation of the VIC model. The implementation of VIC following this procedure has been

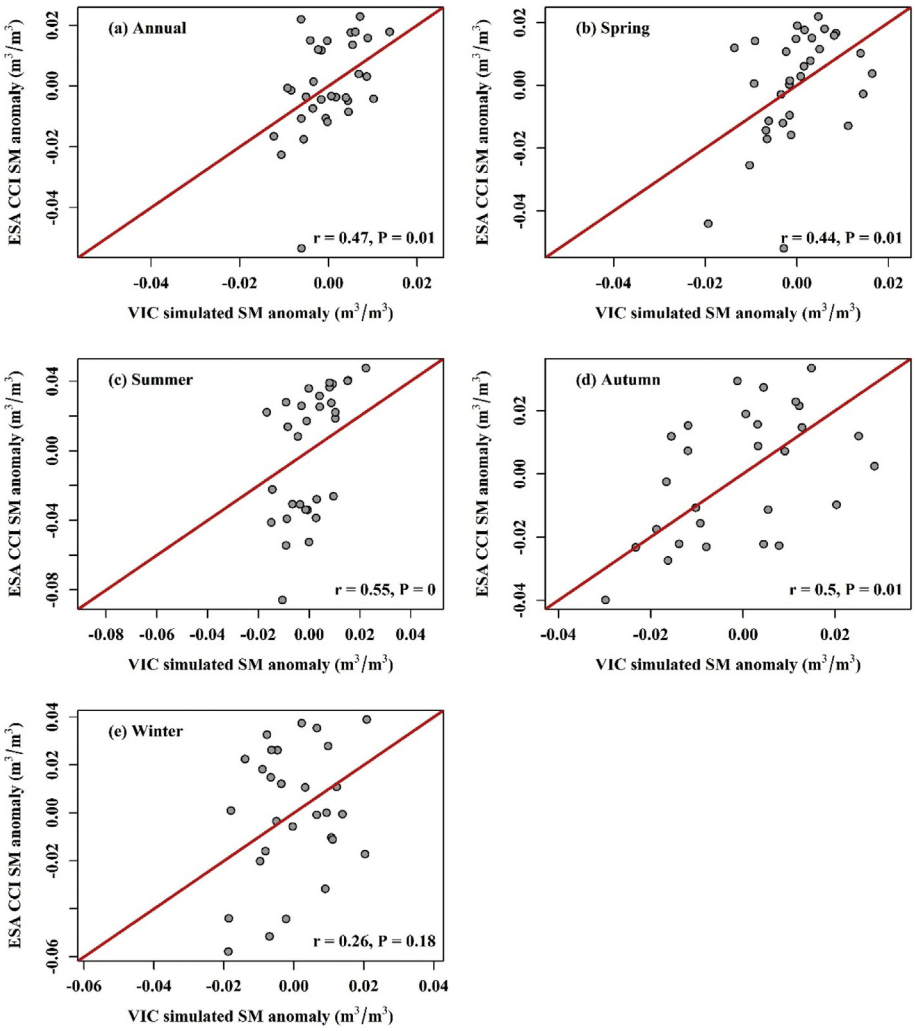

Fig. 4. Scatter plots of the areal means of SM anomaly simulated by the VIC versus those of the ESA CCI (a) of years, (b) in spring, (c) in summer, (d) in autumn, and (e) in winter during 1979–2010. The red line represents 1:1 line. In the subplots, r is the correlation, and P represents the p value of the correlation.

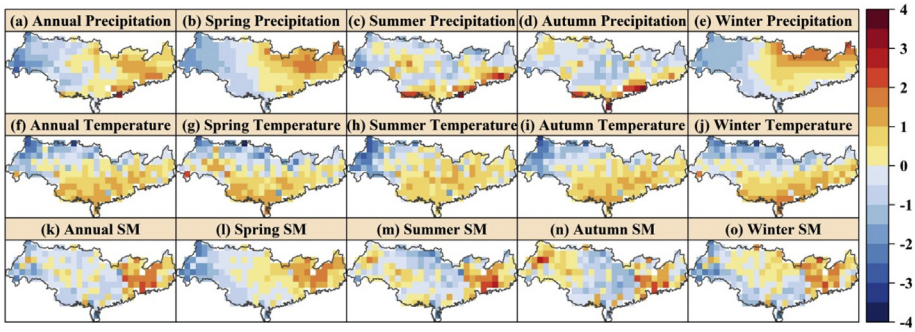

Fig. 5. Spatial distributions of annual and seasonal means in precipitation, temperature and SM across the PRb. The values have been normalized by $(x_i - \bar{x})/\sigma$ over the PRb, where x_i is the value of the ith grid, $\bar{x}$ is the spatial mean of x_i across the PRb, and σ is the standard deviation.

successfully applied in the PRb (e.g. Li et al., 2017).

3.2. Trend detection method

The Mann-Kendall test (M-K test) was used to quantify the significance of the possible trends of a time series (Mann, 1945; Kendall, 1975). As a nonparametric test, the M-K test provides more robust results against outliers and skewed distributions. The M-K test has been widely used in the fields of hydrology, climatology, and meteorology (e.g. Gu et al., 2017a,b; Zhang et al., 2014). The statistic S of the M-K test, defined as the proportion of concordant pairs minus the proportion of discordant pairs in the sample, was used to identify the temporal trend:

$$\begin{cases} S = \sum_{i=1}^{n-1} \sum_{j=i+1}^{N} \mathrm{sgn}(X_j - X_i) \\ \mathrm{sgn}(X_j - X) = \begin{cases} 1 & X_j - X_i > 0 \\ 0 & X_j - X_i = 0 \\ -1 & X_j - X_i < 0 \end{cases} \end{cases} \quad (2)$$

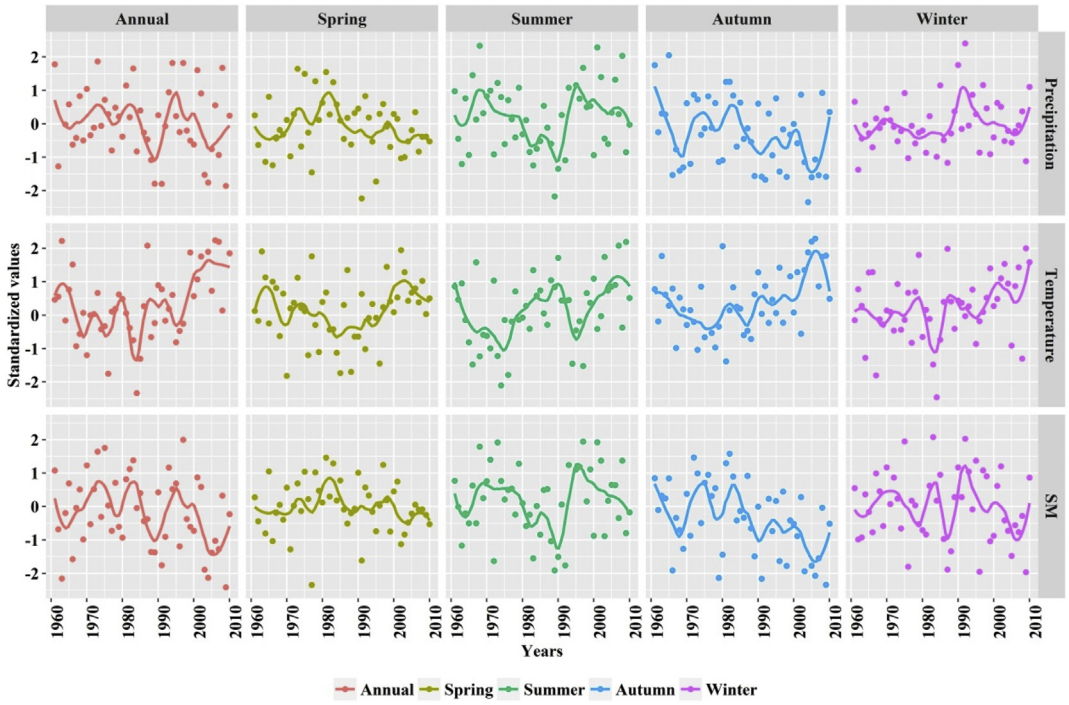

Fig. 6. Temporal changes of annual and seasonal normalized precipitation, temperature and SM across the PRb. The values are normalized by $(x_i - \bar{x})/\sigma$, where x_i is the value of the ith year, $\bar{x}$ is the temporal mean of x_i in 1961–1990, and σ is the standard deviation. The colored curves denote locally weighted smoothing lines (LOESS).

where X_i and X_j are the data values in the time series and n is the size of the sample. The significance of the trend was detected by the M-K test at the significance level of 5%.

Either serial or cross correlation may affect the results of Mann-Kendall test, so pre-whitening procedure was needed to reduce the influences of such correlations (Yue et al., 2002). Finally, the magnitude of trend was calculated by Sen's slope β (Sen, 1968):

$$\beta = \text{median}\left(\frac{X_j - X_i}{j - i}\right) \quad \forall\ i < j \tag{3}$$

3.3. Maximum covariance analysis (MCA)

Maximum covariance analysis (MCA), one type of singular value decomposition (SVD) analyses in the fields of climate and meteorology, has been widely used to detect coupled modes of the variability between two time series (Mo, 2003). MCA constructs a covariance matrix between two datasets and then performs an SVD of the resulting matrix. Let $\mathbf{X}$ be a p-by-n matrix consisting of p variables with n realizations, and $\mathbf{Y}$ be a q-by-n matrix of q variables with n realizations. The SVD of the covariance matrix $\mathbf{C}$ between $\mathbf{X}$ and $\mathbf{Y}$ is calculated (Mo, 2003):

$$\mathbf{C} = \frac{1}{n}\mathbf{X}\mathbf{Y}' = \mathbf{U}_c\mathbf{\Lambda}_c\mathbf{V}_c' \tag{4}$$

where prime denotes the matrix transpose; $\mathbf{\Lambda}_c$ is an r-by-r diagonal matrix of nonnegative singular values λ_i (i = 1, 2, …, r) arranged in descending order, with $r \le \min(p, q, n-1)$ being the rank of $\mathbf{C}$; and $\mathbf{U}_c$ (p-by-r) and $\mathbf{V}_c$ (q-by-r) are column-orthonormal matrices containing the *left* and *right* singular vectors. The total squared covariance in $\mathbf{C}$ is given by the sum of the squared diagonal values of $\mathbf{\Lambda}_c$, and the relative importance of the kth singular mode can be measured in terms of squared covariance fraction, defined as $\lambda_k{}^2/\Sigma\lambda_i{}^2$. Then, two n-by-r matrices of expansion coefficients, $\mathbf{A}_c$ and $\mathbf{B}_c$, can be defined to satisfy the following equations (Mo, 2003):

$$\begin{cases} \mathbf{A}_c = \mathbf{X}'\mathbf{U}_c \\ \mathbf{B}_c = \mathbf{Y}'\mathbf{V}_c \end{cases} \tag{5}$$

where the columns of $\mathbf{A}_c$ and $\mathbf{B}_c$ contain the time series describing how each mode of variability oscillates. MCA has the ability to split the temporal and spatial patterns between two associated variables, and further to extract the coherent patterns of two variables that are most strongly related to each other (Leonardi et al., 2002).

3.4. Contribution analysis

The contributions of precipitation and temperature to soil moisture were detected by multivariate regression methodology, which has been widely used in detection and attribution studies of climate change (e.g. Li et al., 2011; Ting et al., 2009). The regression equation is:

$$S' = a \times P + b \times T + \varepsilon \tag{6}$$

where P and T represent precipitation and temperature, respectively; a and b are regression coefficients; ε is a constant; and S' is the soil moisture predictand, which can be roughly estimated as the soil moisture component jointly affected by precipitation and temperature. Therefore, the change in soil moisture $\Delta S'$ can be estimated by;

$$\Delta S' = a \times \Delta P + b \times \Delta T \tag{7}$$

where $\Delta P'$ and $\Delta T'$ are the changes in precipitation and temperature, respectively. Then based on Eq. (7), the contributions of precipitation and temperature to soil moisture can be calculated by:

$$\begin{cases} CP = (a \times \Delta P)/\Delta S' \times 100\% \\ CT = (b \times \Delta T)/\Delta S' \times 100\% \end{cases} \tag{8}$$

where CP and CT are the contributions of precipitation and temperature to soil moisture, respectively. The contributions of precipitation or temperature to soil moisture can be positive or negative. Based on Eq. (7), the change in soil moisture is only attributed to the changes in precipitation and temperature, so the sum of the contributions of precipitation and temperature to soil moisture should be 100%. Therefore,

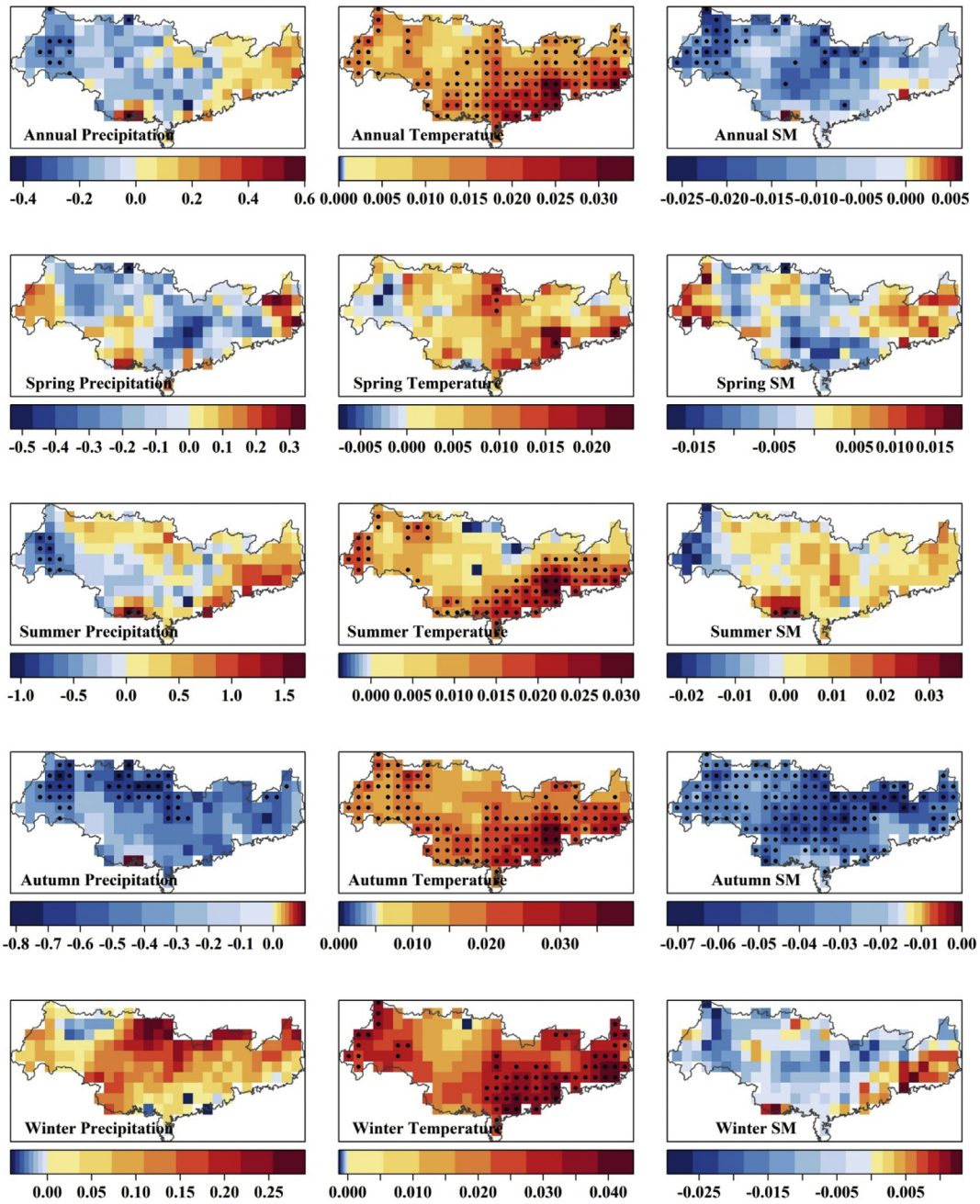

Fig. 7. Spatial distribution of liner trends in annual and seasonal precipitation (mm/y), temperature (°C/y), and SM (mm/y). The marked grids denote the trends are significant in the M-K test at the 95% confidence level.

the relative contributions in percentage of precipitation and temperature *CP′* and *CT′* are calculated as follow:

$$\begin{cases} CP' = \frac{|CP|}{|CP| + |CT|} \times 100\% \\ CT' = \frac{|CT|}{(|CP| + |CT|)} \times 100\% \end{cases} \quad (9)$$

4. Results

4.1. Calibration and validation of the VIC model

The VIC model was calibrated by adjusting the seven parameters mentioned above, including *bi*, D_s, D_m, W_s, d_1, d_2 and d_3, to optimize the objective function which compares the simulated and observed streamflow at Boluo, Shijiao, and Wuzhou during 1961–1970. The calibrated VIC was then validated by the observations of streamflow during 1971–1980. Table 1 shows the optimal parameters for the three basins in the calibrated VIC. The monthly *E* values for three basins are all above 0.9 in the calibration period and above 0.8 in the validation period (Table 2). *B* values generally fall within −0.10 and 0, except those at Shijiao and Wuzhou during the validation period. The comparison of the VIC simulations against observations during the periods of calibration and validation (Fig. 2) shows good agreement with the results in Table 2. The VIC can capture the timing of wet and dry months but tends to underestimate the extremely high streamflow. Overall, the VIC is capable of simulating streamflow in the PRb at both daily and monthly scales.

The soil moisture simulated by the VIC was then assessed by the comparison against the GLDAS-2 outputs based on the NOAH land surface model. The depth of soil moisture from NOAH land surface

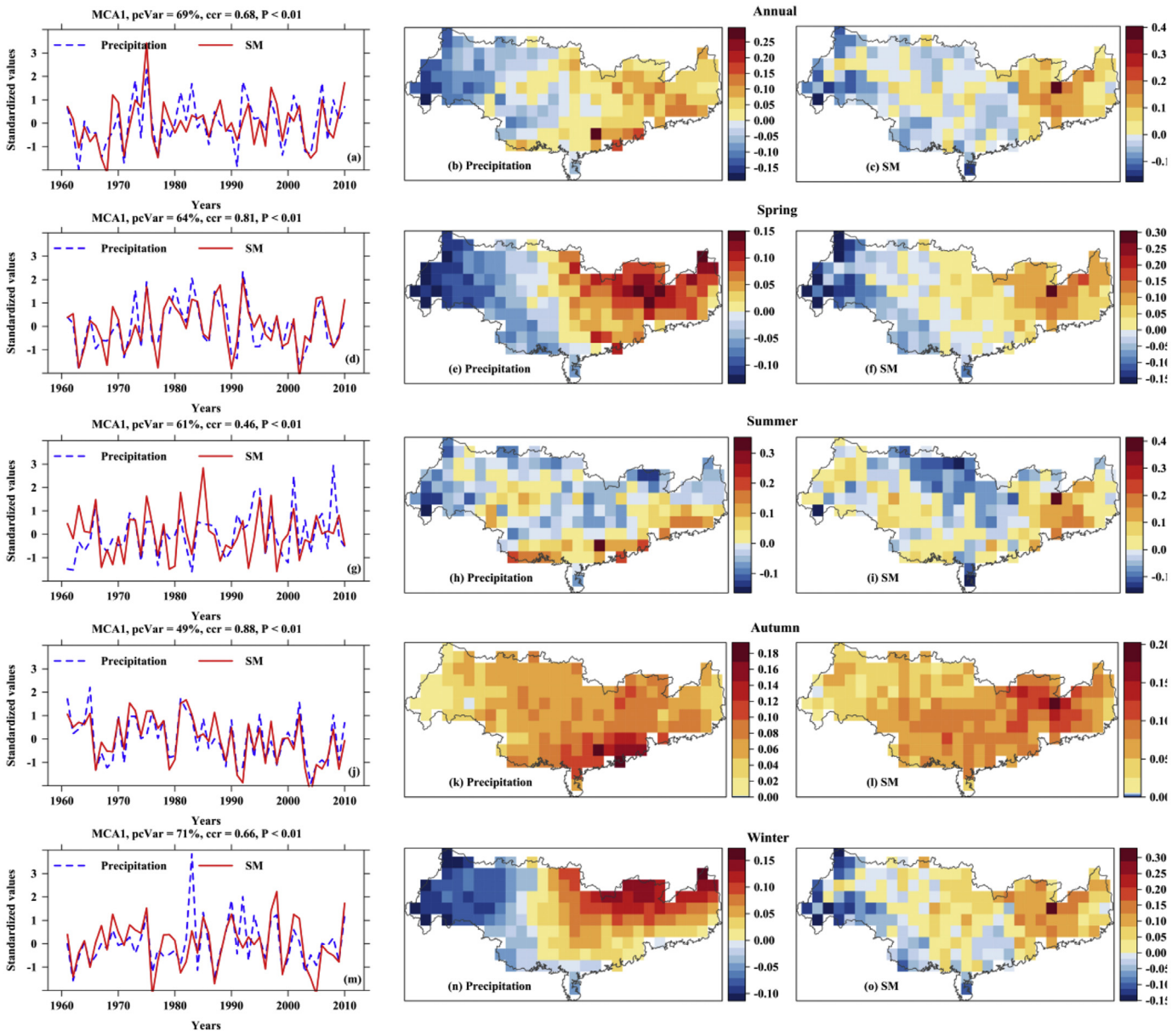

Fig. 8. The temporal and spatial patterns of the first leading MCA mode (MCA1) for annual and seasonal precipitation and SM. Subplots in the first column are the first leading principal component (PC1) time series of precipitation and SM. pcVar denotes the percentage of variance explained by the MCA1, ccr denotes the correlation coefficient between the PC1 of precipitation and SM.

model is 0–10 cm, while the depths from the calibrated VIC are 12, 10, and 13 cm for the East River, North River, and West River basins, respectively. Because depths of soil moisture in different datasets can be different, previous studies usually compared soil moisture values of similar depths from different data sources. For example, Bi et al. (2016) compared observed soil moisture at 0–5 cm against GLDAS Noah simulated soil moisture at 0–10 cm. Given that the differences soil moisture depths between NOAH land surface model and the VIC are not large, the VIC simulated soil moisture are compared against the NOAH simulated values in this study. The relationships of soil moisture anomalies between the VIC simulations and GLDAS-2 NOAH outputs at annual and seasonal scales were used to evaluate the performance of the VIC in simulating soil moisture (Fig. 3). The anomaly was calculated from soil moisture across the entire PRb during 1961–2010 separately the VIC simulations and GLDAS-2 NOAH outputs. At annual and seasonal scales, the soil moisture of the VIC simulations has significant positive correlations with the GLDAS-2 NOAH outputs with correlations larger than 0.8 and p values less than 0.01. Soil moisture anomalies of the VIC and GLDAS-2 NOAH simulations obviously align the 1:1 line. The VIC and GLDAS-2 NOAH simulations are outputs of two different land surface models, i.e. the VIC and NOAH, driven by two different meteorological forcing, i.e. the CMA observation for VIC and the Princeton meteorological dataset for NOAH, the agreement of soil moisture simulations from these two simulations demonstrates the performance of the VIC in simulating soil moisture. The comparison between VIC and ESA CCI anomaly also shows acceptable relationship between these two datasets, although the linear relationships are weaker than those between VIC and GLDAS-2 NOAH (Fig. 4). The positive correlations are positive with statistical significance in annual, spring, summer, and autumn, but that in winter is not significant. Caveat should be made for the comparison between VIC and ESA CCI is that the depths of soil moisture of VIC (i.e. around 10 cm) and ESA CCI (i.e. 0–5 cm) are different.

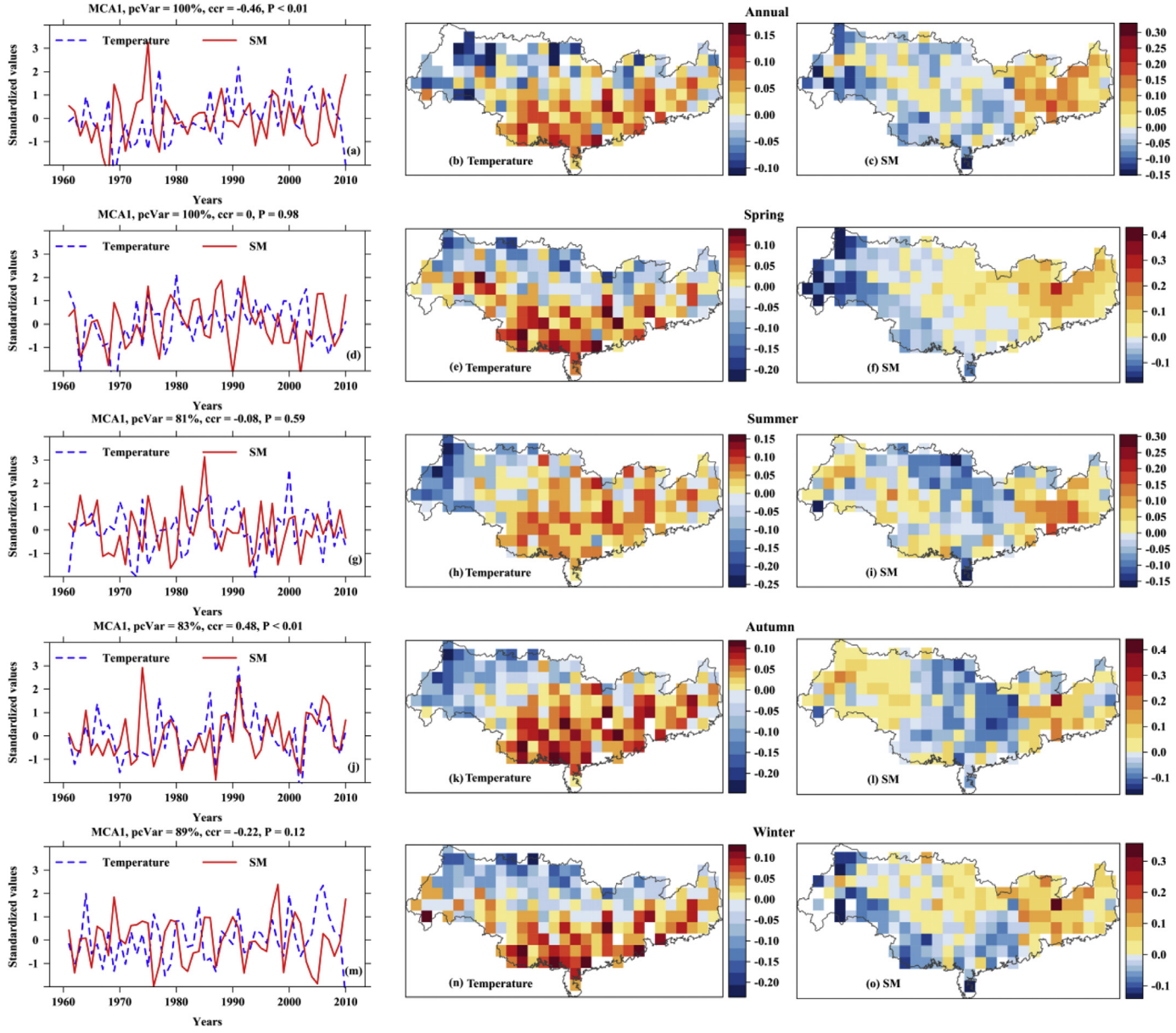

Fig. 9. The same as Fig. 8, but for the temporal and spatial patterns of MCA1 for annual and seasonal temperature and SM.

4.2. Spatiotemporal changes of precipitation, temperature, and soil moisture

Precipitation, temperature, and soil moisture were normalized by their spatial means and standard deviation to remove their differences in magnitudes. The spatial distributions of the normalized precipitation, temperature and soil moisture across the PRb at annual and seasonal scales are shown in Fig. 5. The annual and seasonal normalized soil moisture exhibits different spatial patterns (Fig. 5k–o). Normalized soil moisture is higher in eastern PRb and gradually decreases to lower values in western PRb in spring and winter, but shows a different spatial pattern with higher in eastern and western but lower in central PRb in summer and autumn (Fig. 5l–o). Annual soil moisture is obviously higher in eastern PRb than other regions, which is a combined effect of the spatial distributions of seasonal soil moisture (Fig. 5k).

Overall, compared with temperature, the spatial patterns of annual and seasonal normalized precipitation are in good agreement with those of soil moisture (Fig. 5a–j). Specifically, the areas with high precipitation are mainly in eastern PRb, in which high soil moisture means can be found. This relation between spatial patterns of precipitation and soil moisture is especially obvious for annual, spring and summer (Fig. 5a–e). Annual and seasonal normalized temperature is the highest in southeastern PRb and gradually decreases to northwestern PRb, which is different from the spatial distributions of normalized soil moisture (Fig. 5f–j), implying that temperature may not be the dominant factor of the spatial distributions of soil moisture.

The temporal changes of annual and seasonal normalized precipitation, temperature and soil moisture across the PRb are also showed in Fig. 6. Observational evidence has shown that China has been suffering rapidly temperature increasing (e.g. Li and Ma, 2013; Gu et al., 2017c). In the PRb, during 1961–2010, temperature exhibited fluctuating temporal changes before the 1980s, and then started to increase rapidly afterwards (Fig. 6). Different from the similar temporal changes of the normalized temperature at annual and seasonal scales, the annual and seasonal variabilities of the precipitation show different temporal patterns. The decrease of precipitation can be found after the 1980s for spring, and throughout the period of 1961–2010 for autumn. On the other hand, summer precipitation is relatively low during 1980–1990, but the means before and after this period are comparable.

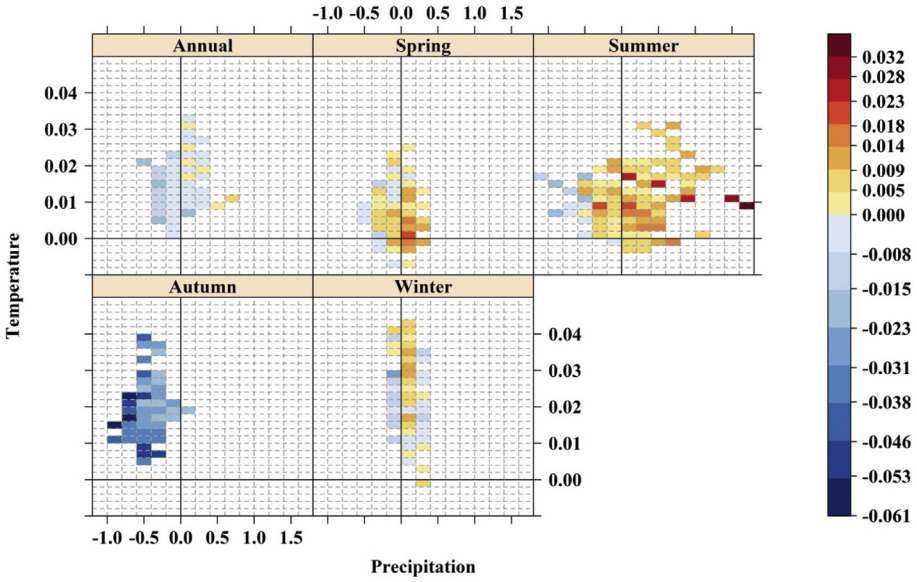

Fig. 10. Trends of SM (mm/y) as a function of precipitation (mm/y) and temperature (°C/y) trends. The colored boxes represent SM trend. The red (blue) boxes are drying (wetting), and blank indicates no data. (For interpretation of the references to colour in this figure legend, the reader is referred to the web version of this article.)

A measurable increase in winter precipitation is detected after the 1980s. Annual precipitation decreases considerably after the late 1990s. Overall, the temporal changes of annual and seasonal precipitation are very similar with those of soil moisture. The soil moisture in autumn decreases more considerably over 1961–2010 than in annual and other seasons, in which the soil moisture fluctuates without measurable trends. Compared to other seasons, the decreasing trend in precipitation and the increasing trend in temperature are more evident in autumn, and soil moisture decreases in a faster rate than precipitation in autumn, indicating the increasing temperature accelerate the speedy decline of soil moisture caused by the decrease in autumn precipitation.

The spatial distributions of trends in precipitation, temperature and soil moisture exhibit obvious spatial heterogeneous (Fig. 7). During the period of 1961–2010, annual and seasonal temperature increases consistently across the whole PRb, and increases the most considerable over the southeastern parts, which are the most urbanized and populated areas in the PRb. Significant increases in temperature are identified in the middle and east parts for annual, the southeast parts for summer, the west and southeast parts for autumn, and the southeast parts for winter, while no significant trends are found in spring. For precipitation, the spatial patterns of temporal trends at annual and seasonal scales are different. The areas with decreasing trends in precipitation are located at the central and west parts for annual, central-east and northwest parts for spring, the southwest parts for summer and the whole PRb for autumn. An increasing winter precipitation trend is identified across the PRb. However, most of the trends in precipitation are insignificant, except for those in the west and north PRb for autumn precipitation. Spatial patterns of trends in precipitation are in good line with those of soil moisture in annual, spring, summer and autumn. The autumn soil moisture is dominated by significantly decreasing trends over almost the whole PRb. In autumn, most of areas experience significant warming and the western and northern parts undergo significant decreases in precipitation, which can explain the significant reduction in the autumn soil moisture. Overall, the above results indicate that precipitation is the dominant factor that largely affects spatiotemporal distributions of soil moisture, and temperature also plays an important role in regulating, especially in the southeastern PRb and autumn.

4.3. Relationships between precipitation, temperature and soil moisture

The MCA analysis was employed to quantitatively identify the coherent patterns between precipitation versus soil moisture, and temperature versus soil moisture (Figs. 8 and 9). The first leading MCA mode (MCA1) of precipitation and soil moisture can explain 69%, 64%, 61%, 49%, and 71% of the variability in annual, spring, summer, autumn and winter, respectively (Fig. 8). The principal component 1 (PC1) of precipitation and soil moisture are significantly correlated with correlation coefficients of 0.68, 0.81, 0.46, 0.88, and 0.66 in annual, spring, summer, autumn and winter, respectively. Furthermore, the spatial patterns of MCA1 precipitation and soil moisture are similar (Fig. 8). Similar to the spatial distributions of changes in precipitation and soil moisture in Fig. 7, the MCA1 in spring and winter exhibit positive trends in eastern PRb and negative trends in western PRb. The result again stresses that precipitation have a primary influence on long-term variability of soil moisture.

Though the MCA1 of temperature and soil moisture can explain at least 81% of total variance (Fig. 9). The correlation coefficients of PC1 of temperature and soil moisture are statistically insignificant, except in annual and autumn. In addition, the spatial patterns of MCA1 also show the negative relation between temperature and soil moisture in annual and autumn (Fig. 9), which in line with their linear trends (Fig. 7). In annual and autumn, areas with increases in temperature are associated with decreases in soil moisture. Therefore, surface warming plays an important role in the changes in soil moisture in annual and autumn, but the impacts of temperature on soil moisture are not significant in spring, summer and winter.

The linear trends of soil moisture were plotted as a function of precipitation and temperature trends simultaneously, which shows the relationship of soil moisture with precipitation and temperature, implying that changes in soil moisture can be partitioned into precipitation-induced and temperature-affected components (Fig. 10). For spring, summer and winter, the trend directions of soil moisture (i.e. drying and wetting) are mainly determined by those of precipitation, indicating that precipitation is a major driver behind trends of soil moisture (Fig. 10). The relationship between temperature and soil moisture is less obvious. Overall, warming temperature is corresponding to soil drying, especially for annual and autumn, despite the magnitude of trend in temperature is irregular to that in soil moisture. In autumn, though decreasing precipitation controls the degree of soil drying, warming temperature amplifies the effects of decreasing precipitation on soil drying. It is also noted that the enhancement of temperature warming on soil drying is complex and unconditional, which can be easily observed in other seasons. The reason why temperature has an unclear relationship with soil moisture is that temperature influences water balance through changing soil

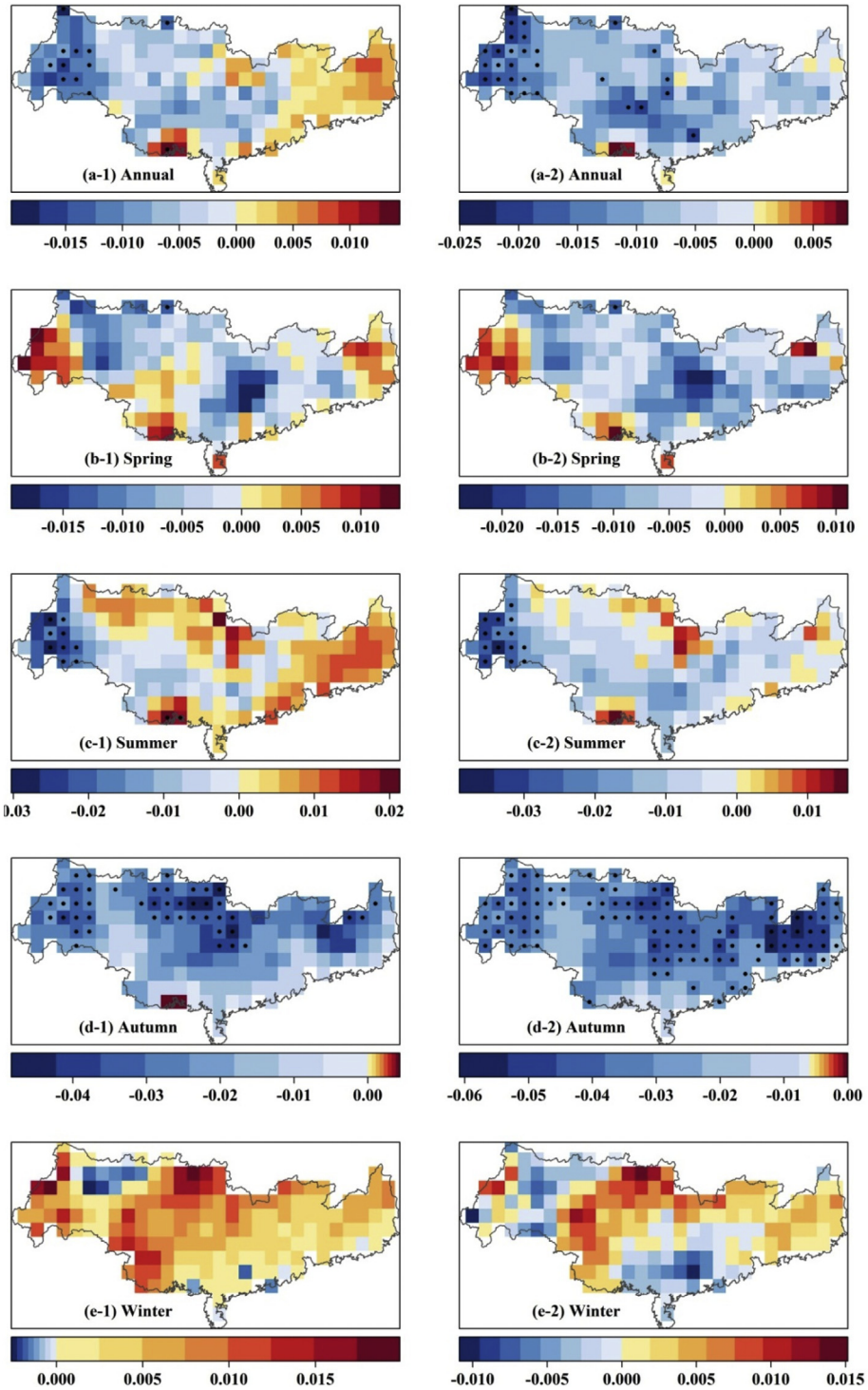

Fig. 11. The spatial distributions of linear trend for SM predictand linearly regressed by precipitation ("-1" in the title of each panel), and precipitation and temperature ("-2" in the title of each panel). The grids marked with black points denote significant trends at the 95% confidence level.

evapotranspiration, further effecting on soil moisture. However, there are many other factors controlling changes in soil evapotranspiration, such as speed, humidity, solar radiation and so on.

4.4. Contributions of precipitation and temperature to soil moisture changes

Although precipitation and temperature are identified as two important factors that largely influence soil moisture changes over PRb, the quantitative effects of precipitation and temperature are still unclear. The multiple linear regression was applied to obtain their contributions (Figs. 11 and 12). Fig. 11 shows the changes in soil moisture predictand (i.e. S' in Eq. (5)) linearly regressed by precipitation only, and precipitation and temperature together, respectively. Compared Fig. 7 and Fig. 11, the spatial patterns of soil moisture predictand linearly regressed by precipitation have high degree of similarity with those of the VIC simulated soil moisture at annual and seasonal scales. However, the magnitudes of trends in soil moisture predictand are smaller than those of soil moisture especially for annual and autumn, due to the trends of precipitation are not significant and the magnitude of trends of precipitation is small (Figs. 7 and 11). When

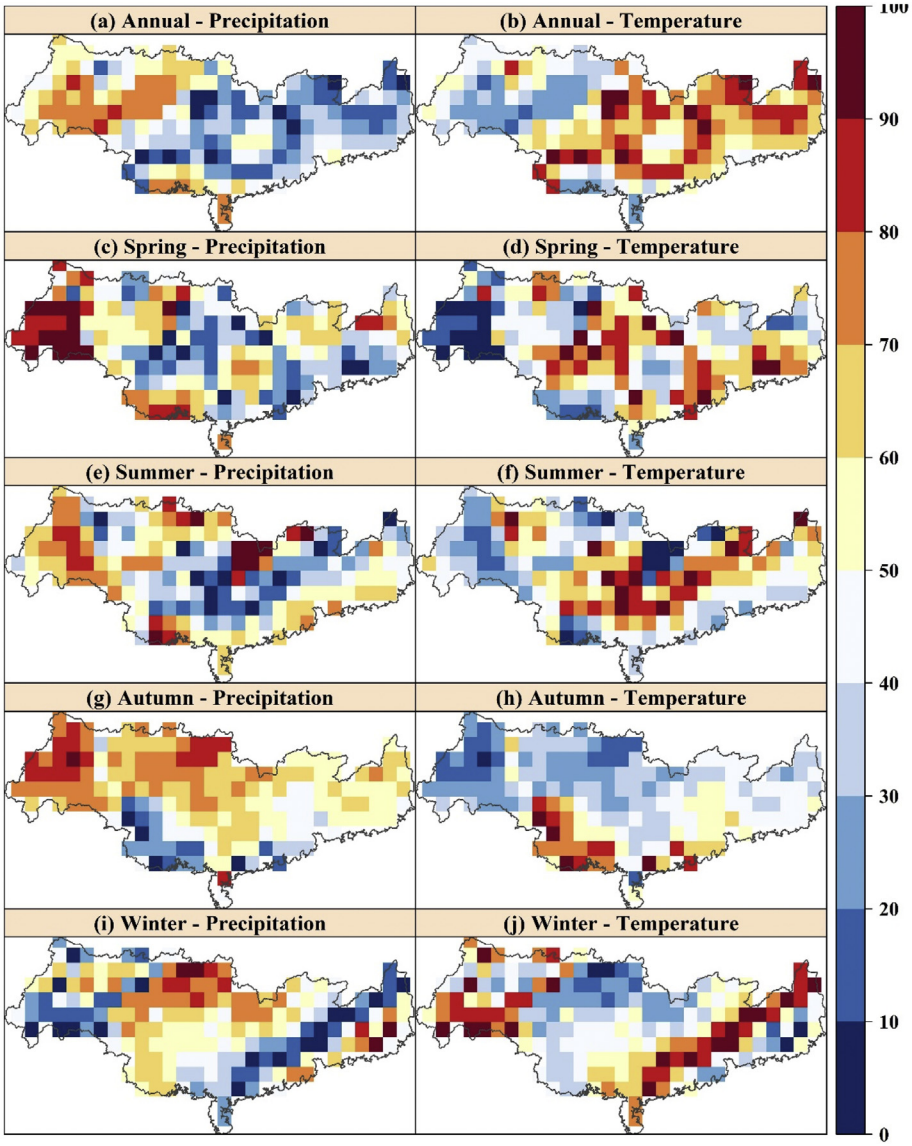

Fig. 12. The relative contributions of precipitation and temperature to changes in SM.

precipitation and temperature are both considered in the regression, there is higher degree of similarities between spatial patterns of trends in soil moisture predictand and soil moisture. Moreover, with consideration of temperature changes, some areas with wetting soil moisture predictand change to get drying, and the magnitude of drying trends in soil moisture predictand becomes much more significant. These results further demonstrate the enhancement effect of increasing temperature on soil moisture drying.

Fig. 12 shows the fractional contributions of precipitation and temperature to soil moisture changes. At annual and seasonal scales, these contributions showed obviously spatial heterogeneity. Additionally, there are clearly differences in spatial patterns of contributions among annual and seasonal scales. In general, except for winter, precipitation is the dominant factor for changes in soil moisture over western PRb with contributions larger than 70%. The areas with temperature as dominant contribution factor are central-eastern Pearl River, except for autumn. Autumn is a long-term drying soil season at which the contributions of precipitation and temperature over central-eastern PRb were roughly equivalent.

5. Discussions and conclusions

Daily soil moisture at the spatial 0.5° × 0.5° resolution was simulated by the VIC hydrological model forced by the gridded climatic factors. The simulations of streamflow and soil moisture were assessed by comparing with the observations from major hydrological stations and outputs of GLDAS-2 NOAH. The spatiotemporal changes in annual and seasonal soil moisture during 1961–2010 were estimated based on the M-K trend test. The relations of changes in soil moisture and changes in its controlling factors, including precipitation and temperature, were qualitatively and quantitatively assessed by the MCA analysis to understand the mechanisms of changes in soil moisture in different seasons. The following conclusions can be drawn from the results:

(1) The VIC is capable of simulating daily streamflow and soil moisture in the PRb. The temporal changes and variability of simulated soil moisture highly resemble those of hydrological observations and GLDAS-2 NOAH. During 1961–2010, the average soil moisture is generally higher in the eastern parts of the PRb. The average soil moisture shows different spatial pattern in the four seasons. In spring, soil moisture decreases from the eastern to the western

parts, but in summer, soil moisture is higher in the eastern and western parts compared to the middle PRb.

(2) The spatiotemporal changes in soil moisture during 1961–2010 exhibit various patterns in different seasons. The decreases in annual soil moisture are insignificant in the PRb, which is in good agreement with previous studies mostly focusing on annual changes in soil moisture in a larger study area, e.g. East Asia in Cheng et al. (2015) and eastern China in Chen et al. (2015). However, our results at seasonal scale indicate a statistically significant drying trend in soil moisture over the PRb in autumn. Since autumn is the season of agricultural harvest in the PRb, drying autumn suggests increasing risks of agricultural droughts and reductions in agricultural production, which is hardly identified in previous studies at the annual scale. In spring and summer, increases in soil moisture are detected in the eastern and the whole PRb, respectively.

(3) The relations between changes in soil moisture and their controlling factors in the four seasons, i.e. precipitation and temperature, are assessed by the comparison of temporal change and spatial patterns. The significant reduction in precipitation combined with substantial increase in temperature is the major reason of the drying in autumn soil moisture. In most cases, the changing directions of soil moisture resemble those of precipitation, suggesting that precipitation is the key factors that affect soil moisture. However, in winter, soil moisture changes negligibly even though precipitation increases. The contradict change directions are due to the significant increase in temperature.

(4) The first leading MCA mode can explain most of the coherent variability of precipitation and temperature, and the temporal changes of the MCA1 of soil moisture are highly and significantly correlated with those of precipitation. On the other hand, the temporal changes of the MCA1 of temperature have significant relations with soil moisture in annual and autumn. In general, the increases in temperature aggregate the drying of soil moisture. Trends of soil moisture predicted by the linear regression with considerations of precipitation and temperature are generally smaller than those predicted by precipitation only. Additionally, besides precipitation and temperature, soil moisture is also influenced by other factors, such as land cover/use changes, landscape features, and irrigation and urban expansion (Chen et al., 2016a), which may disturb the relationships between soil moisture and precipitation, temperature. However, such anthropogenic factors have less seasonality compare to the climatic variables.

Acknowledgements

The work described in this paper was supported by the grant from the Research Grants Council of the Hong Kong Special Administrative Region, China (*Project No.HKBU22301916*), the Faculty Research Grant from Hong Kong Baptist University (*Project No.FRG2/15-16/043*), National Science Foundation for Distinguished Young Scholars of China (No. 51425903), Creative Research Groups of National Natural Science Foundation of China (Grant No.: 41621061), the Strategic Priority Research Program Grant of the Chinese Academy of Sciences (Grant No. XDA19070402), and the Fundamental Research Funds for the Central Universities, China University of Geosciences (Wuhan) (Grant No. CUG180614). Observed daily precipitation and temperature are available at the National Meteorological Information Center for the China Meteorological Administration at http://www.cma.gov.cn/2011qxfw/2011qsjgx/.

References

Bastiaanssen, W., 2000. SEBAL-based sensible and latent heat fluxes in the irrigated Gediz Basin, Turkey. J. Hydro. 229 (1), 87–100.

Bi, H., Ma, J., Zheng, W., Zeng, J., 2016. Comparison of soil moisture in GLDAS model simulations and in situ observations over the Tibetan Plateau. J. Geophys. Res. Atmos. 121, 2658–2678.

Chen, Y., Yang, K., Qin, J., Zhao, L., Tang, W., Han, M., 2013. Evaluation of AMSR-E retrievals and GLDAS simulations against observations of a soil moisture network on the central Tibetan Plateau. J. Geophys. Res. Atmos. 118, 4466–4475.

Chen, X., Su, Y., Liao, J., Shang, J., Dong, T., Wang, C., Liu, W., Zhou, G., Liu, L., 2016a. Detecting significant decreasing trends of land surface soil moisture in eastern China during the past three decades (1979–2010). J. Geophys. Res. Atmos. 121, 5177–5192.

Chen, Y.D., Zhang, Q., Xiao, M.Z., Singh, V.P., Zhang, S., 2016b. Probabilistic forecasting of seasonal droughts in the Pearl River basin, China. Stoch. Env. Res. Risk A. 30 (7), 2031–2040.

Cherkauer, K.A., Lettenmaier, D.P., 2003. Simulation of spatial variability in snow and frozen soil. J. Geophys. Res. Atmos. 108 (D22). http://dx.doi.org/10.1029/2003JD003575.

Cheng, S., Guan, X., Huang, J., Ji, F., Guo, R., 2015. Long-term trend and variability of soil moisture over East Asia. Journal of Geophysical Research: Atmospheres 120, 8658–8670.

Dai, A., 2013. Increasing drought under global warming in observations and models. Nat. Clim. Chang. 3 (1), 52–58.

Dan, L., Ji, J., Xie, Z., Chen, F., Wen, G., Richey, J.E., 2012. Hydrological projections of climate change scenarios over the 3H region of China: a VIC model assessment. J. Geophys. Res. Atmos. 117http://dx.doi.org/10.1029/2011JD017131. D11102.

Dorigo, W., Jeu, R., Chung, D., Parinussa, R., Liu, Y., Wagner, W., Fernandez-Prieto, D., 2012. Evaluating global trends (1988–2010) in harmonized multi-satellite surface soil moisture. Geophys. Res. Lett. 39, L18405. http://dx.doi.org/10.1029/2012GL052988.

Ducoudre, N.I., Laval, K., Perrier, A., 1993. SECHIBA, a new set of parameterizations of the hydrologic exchanges at the land-atmosphere interface within the LMD atmospheric general circulation model. J. Clim. 6 (2), 48–273.

Feng, H., 2016. Individual contributions of climate and vegetation change to soil moisture trends across multiple spatial scales. Sci. Rep. 6, 32782. http://dx.doi.org/10.1038/srep32782.

Fischer, E.M., Seneviratne, S.I., Vidale, P.L., Luthi, D., Schar, C., 2007. Soil moisture-atmosphere interactions during the 2003 European summer heat wave. J. Clim. (20), 5081–5099.

Gao, H., Tang, Q., Shi, X., Zhu, C., Bohn, T., Su, F., Sheffeld, J., Pan, M., Lettenmaier, D., Wood, E.F., 2010. Water budget record from variable infltration capacity (VIC) model. In Algorithm Theoretical Basis Document for Terrestrial Water Cycle Data Records.

Gu, X., Zhang, Q., Singh, V.P., Xiao, M., Chen, J., 2017a. Nonstationarity-based evaluation of flood risk in the Pearl River basin: changing patterns, causes and implications. Hydrol. Sci. J. 62, 246–258.

Gu, X., Zhang, Q., Singh, V.P., Liu, L., Shi, P., 2017b. Spatiotemporal patterns of annual and seasonal precipitation extreme distributions across China and potential impact of tropical cyclones. Int. J. Climatol. http://dx.doi.org/10.1002/joc.4969.

Gu, X., Zhang, Q., Singh, V.P., Shi, P., 2017c. Changes in magnitude and frequency of heavy precipitation across China and its potential links to summer temperature. J. Hydrol. 547, 718–731.

Hansen, M.C., Defries, R., Townshend, J.R.G., Sohlberg, R., 2000. Global land cover classifcation at 1 km spatial resolution using a classifcation tree approach. Int. J. Remote Sens. 21, 1331–1364.

IPCC, 2013. Climate change 2013: The physical science basis. In: Contribution of Working Group 1 to the Fifth Assessment Report of the Intergovernmental Panel on Climate Change. Cambridge University Press, Cambridge, UK and New York, NY.

Kalnay, E., Kanamitsu, M., Kistler, R., Collins, W., Deaven, D., Gandin, L., Iredell, M., Saha, S., White, G., Woollen, J., Zhu, Y., Leetmaa, A., Reynolds, R., Chelliah, M., Ebisuzaki, W., Higgins, W., Janowiak, J., Mo, K.C., Ropelewski, C., Wang, J., Jenne, R., Joseph, D., 1996. The NCEP/NCAR 40-Year Reanalysis Project. Bull. Am. Meteorol. Soc. 77, 437–471.

Kendall, M.G., 1975. Rank Correlation Methods. Griffin, London.

Koster, R.D., Dirmeyer, P.A., Guo, Z., Bonan, G., Chan, E., Cox, P., Gordon, C.T., Kanae, S., Kowalczyk, E., Lawrence, D., Liu, P., Lu, C.-H., Malyshev, S., McAvaney, B., Mitchell, K., Mocko, D., Oki, T., Oleson, K., Pitman, A., Sud, Y.C., Taylor, C.M., Verseghy, D., Vasic, R., Xue, Y., Yamada, T., 2004. Regions of strong coupling between soil moisture and precipitation. Science 305, 1138–1140.

Lawrence, D., Vandecar, K., 2014. Effects of tropical deforestation on climate and agriculture. Nat. Clim. Chang. 5, 27–36.

Leonardi, A.P., Morey, S.L., O'Brien, J.J., 2002. Interannual variability in the eastern subtropical North Pacific Ocean. J. Phys. Oceanogr. 32, 1824–1837.

Li, M., Ma, Z., 2013. Soil moisture-based study of the variability of dry-wet climate and climate zones in China. Chin. Sci. Bull. 58 (4–5), 531–544.

Li, G., Ren, B., Zheng, J., Yang, C., 2011. Net air–sea surface heat flux during 1984–2004 over the North Pacific and North Atlantic oceans (10°N–50°N): annual mean climatology and trend. Theor. Appl. Climatol. 104 (3–4), 387–401.

Li, J., Zhang, Q., Chen, Y.D., Singh, V.P., 2013a. GCMs-based spatiotemporal evolution of climate extremes during the 21st century in China. Journal of Geophysical Research: Atmospheres 118, 11017–11035.

Li, J., Zhang, Q., Chen, Y.D., Xu, C.-Y., Singh, V.P., 2013b. Changing spatiotemporal patterns of precipitation extremes in China during 2071-2100 based on Earth System Models. Journal of Geophysical Research: Atmospheres 118, 12537–12555.

Li, J., Zhang, Q., Chen, Y.D., Singh, V.P., 2015. Future joint probability behaviors of precipitation extremes across China: spatiotemporal patterns and implications for flood and drought hazards. Glob. Planet. Chang. 124, 107–122.

Li, J., Zhang, L., Shi, X., Chen, Y.D., 2017. Response of long-term water availability to more extreme climate on the Pearl River Basin, China. Int. J. Climatol. 37 (7), 3223–3237.

Liang, X., Lettenmaier, D.P., Wood, E.F., Burges, S.J., 1994. A simple hydrologically based

model of land surface water and energy fluxes for general circulation models. Journal of Geophysical Research: Atmospheres 99, 14415–14428.
Lin, B., Stackhouse, P.W., Minnis, P., Wielicki, B.A., Hu, Y., Sun, W., Fan, T.F., Hinkelman, L.M., 2008. Assessment of global annual atmospheric energy balance from satellite observations. J. Geophys. Res. 113, D16114. http://dx.doi.org/10.1029/2008JD009869.
Liu, Y.Y., Parinussa, R.M., Dorigo, W.A., De Jeu, R.A.M., Wagner, W., Van Dijk, A.I.J.M., et al., 2011. Developing an improved soil moisture dataset by blending passive and active microwave satellite-based retrievals. Hydrol. Earth Syst. Sci. 15, 425–436.
Liu, Y.Y., Dorigo, W.A., Parinussa, R.M., De Jeu, R.A.M., Wagner, W., McCabe, M.F., et al., 2012. Trend-preserving blending of passive and active microwave soil moisture retrievals. Remote Sens. Environ. 123, 280–297.
Lohmann, D., Raschke, E., Nijssen, B., Lettenmaier, D.P., 1998. Regional scale hydrology: I. Formulation of the VIC-2L model coupled to a routing model. Hydrol. Sci. J. 43, 131–141.
Mann, H.B., 1945. Nonparametric tests against trend. Econometrica 13, 245–259.
Mo, R., 2003. Efficient algorithms for maximum covariance analysis of datasets with many variables and fewer realizations: a revisit. J. Atmos. Ocean. Technol. 20, 1804–1809.
Niu, J., Chen, J., 2010. Terrestrial hydrological features of the Pearl River basin in South China. J. Hydro Environ. Res. 4 (4), 279–288.
Niu, J., Chen, J., Sivakumar, B., 2014. Teleconnection analysis of runoff and soil moisture over the Pearl River basin in southern China. Hydrol. Earth Syst. Sci. 18, 1475–1492.
Nijssen, B.N., O'Donnell, G.M., Lettenmaier, D.P., Lohmann, D., Wood, E.F., 2001a. Predicting the discharge of global rivers. J. Clim. 14 (15), 3307–3323.
Nijssen, B.N., O'Donnell, G.M., Hamlet, A.F., Lettenmaier, D.P., 2001b. Hydrologic sensitivity of global rivers to climate change. Clim. Change 50, 143–175.
Pearl River Water Resources Committee (PRWRC), 1991. The Zhujiang Archive. Vol. 1 Guangdong Science and Technology Press, Guangzhou (in Chinese).
Rodell, M., Houser, P.R., Jambor, U., Gottschalck, J., Mitchell, K., Meng, C.-J., Arsenault, K., Cosgrove, A., Radakovich, J., Bosilovich, M., Entin, J.K., Walker, J.P., Lohmann, D., Toll, D., 2004. The global land data assimilation system. Bull. Amer. Meteor. Soc. 85 (3), 381–394.
Rui, H., Beaudoing, H., 2016. README Document for Global Land Data Assimilation System Version 2 (GLDAS-2) Products.
Sen, P.K., 1968. Estimates of the regression coefficient based on Kendall's Tau. J. Am. Stat. Assoc. 63 (324), 1379–1389.
Seto, K.C., Woodcock, C.E., Song, C., Huang, X., Lu, J., Kaufmann, R.K., 2002. Monitoring land-use change in the Pearl River Delta using Landsat TM. Int. J. Remote Sens. 23 (10), 1985–2004.
Senevirate, S.I., Corti, T., Davin, E.L., Hirschi, M., Jaeger, E.B., Lehner, I., Orlowsky, B., Teuling, A.J., 2010. Investigating soil moisture interactions in a changing climate: a review. Earth Sci. Rev. 99 (3), 125–161.
Sillmann, J., Kharin, V.V., Zwiers, F.W., Zhang, X., Bronaugh, D., 2013a. Climate extremes indices in the CMIP5 multimodel ensemble: part 1: model evaluation in the present climate. J. Geophys. Res. Atmos. 118, 1716–1733.
Shuttleworth, W.J., 1993. Evaporation, in Handbook of Hydrology. McGraw-Hill, Inc., New York, NY.
Shi, X., Wood, A.W., Lettenmaier, D.P., 2008. How essential is hydrologic model calibration to seasonal streamflow forecasting? J. Hydrometeorol. 9, 1350–1363.
Sillmann, J., Kharin, V.V., Zwiers, F.W., Zhang, X., Bronaugh, D., 2013b. Climate extremes indices in the CMIP5 multimodel ensemble: part 2. Future climate projections. J. Geophys. Res. Atmos. 118, 2473–2493.
Sivapalan, M., Woods, R.A., Kalma, J.D., 1997. Variable bucket representation of TOPMODEL and investigation of the effects of rainfall heterogeneity. Hydrol. Process. 11 (9), 1307–1330.
Syed, T., Famiglietti, J., Rodell, M., Chen, J., Wilson, C., 2008. Analysis of terrestrial water storage changes from GRACE and GLDAS. Water Resour. Res. 44, W02433. http://dx.doi.org/10.1029/2006WR005779.
Ting, M., Kushnir, Y., Seager, R., Li, C., 2009. Forced and internal twentieth-century SST trends in the North Atlantic. J. Clim. 22 (6), 1469–1481.
Wang, X., Wu, H., Dai, K., Zhang, D., Feng, Z., Zhao, Q., Wu, X., Jin, K., Cai, D., Oenema, O., Hoogmoed, W.B., 2012. Tillage and crop residue effects on rainfed wheat and maize production in northern China. Field Crop Res. 132, 106–116.
Wu, Z.Y., Lu, G., Wen, L., Lin, C.A., Zhang, J., Yang, Y., 2007. Thirty-fve year (1971–2005) simulation of daily soil moisture using the variable infltration capacity model over China. Atmos. Ocean 45 (1), 37–45.
Xie, Z., Yuan, F., Duan, Q., Zheng, J., Liang, M., Chen, F., 2007. Regional parameter estimation of the VIC land surface model: methodology and application to river basins in China. J. Hydrometeorol. 9, 1350–1363.
Yan, D., Werners, S.E., Ludwig, F., Huang, H.Q., 2015. Hydrological response to climate change: the Pearl River, China under different RCP scenarios. Journal of Hydrology: Regional Studies 4, 228–245.
Yang, K., Koike, T., Kaihotsu, I., Qin, J., 2009. Validation of a dual-pass microwave land data assimilation system for estimating surface soil moisture in semiarid regions. J. Hydrometeorol. 10 (3), 780–793.
Yang, K., He, J., Tang, W., Qin, J., Cheng, C.C.K., 2010. On downward shortwave and longwave radiations over high altitude regions: observation and modelling in the Tibetan Plateau. Agric. Forest. Meteorol. 150, 38–46.
Yue, S., Pilon, P., Phinney, B., Cavadias, G., 2002. The influence of autocorrelation on the ability to detect trend in hydrological series. Hydrol. Process. 16, 1807–1829.
Zhang, J., Wang, W.C., Wei, J., 2008. Assessing land-atmosphere coupling using soil moisture from the Global Land Data Assimilation System and observational precipitation. J. Geophys. Res. 113, D17119. http://dx.doi.org/10.1029/2008JD009807.
Zhang, Q., Xu, C.-Y., Becker, S., Zhang, Z.X., Chen, Y.D., Coulibaly, M., 2009. Trends and abrupt changes of precipitation maxima in the Pearl River basin. Atmos. Sci. Let. 10, 132–144.
Zhang, Q., Singh, V.P., Li, J., Chen, X., 2011a. Analysis of the periods of maximum consecutive wet days in China. J. Geophys. Res. Atmos. 116, D23106.
Zhang, Q., Chen, Y.D., Chen, X., Li, J., 2011b. Copula-based analysis of hydrological extremes and implications of hydrological behaviors in the Pearl River basin, China. J. Hydrol. Eng. 16 (7), 598–607.
Zhang, Q., Li, J., Singh, V.P., Bai, Y., 2012a. SPI-based evaluation of drought events in Xinjiang, China. Nat. Hazards 64 (1), 481–492.
Zhang, Q., Singh, V.P., Peng, J., Chen, Y.D., Li, J., 2012b. Spatial-temporal changes on precipitation structure across the Pearl River basin, China. J. Hydrol. 440, 113–122.
Zhang, Q., Gu, X., Singh, V.P., Xiao, M., Xu, C.-Y., 2014. Stationarity of annual flood peaks during 1951–2010 in the Pearl River basin, China. J. Hydrol. 519, 3263–3274.
Zhao, R.-J., 1992. The Xinanjiang model applied in China. J. Hydrol. 135 (1–4), 371–381.
Ziegler, A.D., Sheffield, J., Maurer, E.P., Nijssen, B., Wood, E.F., Lettenmaier, D.P., 2003. Detection of intensification in global- and continental-scale hydrological cycles: temporal scale of evaluation. J. Clim. 16, 535–547.